



TREK-1 Null Impairs Neuronal Excitability, Synaptic Plasticity, and Cognitive Function

Wei Wang^{1,2} · Conrad M. Kiyoshi¹ · Yixing Du¹ · Anne T. Taylor¹ · Erica R. Sheehan¹ · Xiao Wu¹ · Min Zhou¹

Received: 10 September 2019 / Accepted: 30 October 2019 / Published online: 15 November 2019
© Springer Science+Business Media, LLC, part of Springer Nature 2019

Abstract

TREK-1, a two-pore-domain K⁺ channel, is highly expressed in the central nervous system. Although aberrant expression of TREK-1 is implicated in cognitive impairment, the cellular and functional mechanism underlying this channelopathy is poorly understood. Here we examined TREK-1 contribution to neuronal morphology, excitability, synaptic plasticity, and cognitive function in mice deficient in TREK-1 expression. TREK-1 immunostaining signal mainly appeared in hippocampal pyramidal neurons, but not in astrocytes. TREK-1 gene knockout (TREK-1 KO) increases dendritic sprouting and the number of immature spines in hippocampal CA1 pyramidal neurons. Functionally, TREK-1 KO increases neuronal excitability and enhances excitatory and inhibitory postsynaptic currents (EPSCs and IPSCs). The increased EPSCs appear to be attributed to an increased release probability of presynaptic glutamate and functional expression of postsynaptic AMPA receptors. TREK-1 KO decreased the paired-pulse ratio and severely occluded the long-term potentiation (LTP) in the CA1 region. These altered synaptic transmission and plasticity are associated with recognition memory deficit in TREK-1 KO mice. Although astrocytic expression of TREK-1 has been reported in previous studies, TREK-1 KO does not alter astrocyte membrane K⁺ conductance or the syncytial network function in terms of syncytial isopotentiality. Altogether, TREK-1 KO profoundly affects the cellular structure and function of hippocampal pyramidal neurons. Thus, the impaired cognitive function in diseases associated with aberrant expression of TREK-1 should be attributed to the failure of this K⁺ channel in regulating neuronal morphology, excitability, synaptic transmission, and plasticity.

Keywords TREK-1 (tandem of pore domain in a weak inwardly rectifying K⁺ channel (Twik)-related K⁺ channels) · Hippocampus · Synaptic transmission · Synaptic plasticity · Cognitive impairment

Introduction

TREK-1 (tandem of pore domain in a weak inwardly rectifying K⁺ channel (Twik)-related K⁺ channels) is one of the K⁺ channels in the two-pore-domain potassium channel (K2P) family. TREK-1 shows high expression across the brain from the cortex, hippocampus to the spinal cord [1]. As a leak type K⁺ channel, TREK-1 plays a role in setting the neuronal resting potential and regulating neuronal excitability [2–4]. Additionally, TREK-1 is also highly interactive with the

interstitial environment. For example, the TREK-1 channel activity can be modulated by neuroprotective fatty acids, mechanical stretch, temperature, and pH [3, 5].

TREK-1 shows a unique pattern of expression on both pre- and post-synaptic sites, which allows the channel activity to be modulated by a variety of neuronal neurotransmitter receptors [4, 6]. Evidently, TREK-1 activity can be enhanced by stimulation of G_i-coupled, γ -aminobutyrate type B receptor (GABA_BR) through PKA inhibition [7]. On the contrary, TREK-1 channel activity can be inhibited by G_q-coupled mGluR1/mGluR5 via PKC phosphorylation, G_s-coupled serotonin (5-HT₄R), and β ₂ noradrenaline receptor (β ₂-AR) via PKA-dependent phosphorylation [4]. The synaptic presence of TREK-1 implies the role of this channel in regulating neurotransmission and plasticity. Indeed, TREK-1 deletion increases the level of 5-HT neurotransmission in the hippocampal CA3 region [8]. Also, pharmacological inhibition of TREK-1 alters CaMKIII inhibitor-induced chemical LTP in the hippocampus [9]. Nevertheless, a systematic

✉ Min Zhou
zhou.787@osu.edu

¹ Department of Neuroscience, Ohio State University Wexner Medical Center, Columbus, OH 43210, USA

² Department of Physiology, School of Basic Medicine, Tongji Medical College, Huazhong University of Science and Technology, Wuhan, China

evaluation of the TREK-1 contribution to neuronal excitability, synaptic transmission, and cognitive function remains unavailable.

The pathological role of TREK-1 has attracted increasing attention in various diseases. For example, TREK-2 and TRAAK are the other two neuronal K₂Ps with similar biophysical properties to TREK-1; however, a depression-resistant phenotype could only be induced in TREK-1-deficient mice [8, 10]. Genetic deletion of TREK-1 substantially increases the susceptibility of animals to ischemia and epilepsy insults [11]. Additionally, altered expression of TREK-1 has been implicated as a cause of cognitive impairment associated with postoperative cognitive dysfunction induced by volatile anesthetics [12]. A profound involvement of TREK-1 in neurological disorders further reiterates the importance of this unique K⁺ channel in brain function.

In the present study, we examined the impact of TREK-1 null on neuronal structure, excitability, synaptic transmission, and hippocampal-dependent learning and memory. We show that TREK-1 gene deficiency alters dendritic sprouting and spines in CA1 pyramidal neurons. TREK-1 null also alters neuronal excitability, synaptic transmission, and plasticity. These TREK-1 deficiency-induced alterations at the cellular levels are associated with hippocampal memory deficits.

Materials and Methods

Origin and Source of the Animals

TREK-1 gene (*Kcnk2*) knockout (TREK-1 KO) mice were generated on a mixed background of C57BL6J and SV129 strains. Prior to this study, this TREK-1 KO line has been backcrossed with C57BL6J for more than ten generations in our laboratory. In this *kcnk2* mutant, a 4-kbp genomic DNA sequence between exon 2 and intron 3 was replaced by a β -galactosidase/neomycin (*LacZ/Neo*) selection cassette [13]. C57BL6J mice were used in control experiments. In some experiments, BAC *Aldh111-eGFP* transgenic reporter mice were used for visualization of astrocytes [14]. Mice of both sexes at postnatal day (P) of 21–28 were used. Mice were anesthetized using chloral hydrate (Sigma-Aldrich, St. Louis, MO, USA) prior to decapitation. All the mice were housed in a 12-h light/dark cycle at the temperature-controlled environment (22 ± 2 °C) with access to food and water ad libitum. All the TREK-1 KO mice used in the experiments have confirmed the deletion of *Kcnk2* gene by PCR genotyping, as performed in our previous study [15].

Electrophysiology

Acute horizontal hippocampal slices (250 μ m) were prepared as previously described [16]. For astrocyte recording, slices

were maintained at room temperature in aCSF containing the following (in mM): 125 NaCl, 25 NaHCO₃, 1.25 NaH₂PO₄, 3.5 KCl, 2 CaCl₂, 1 MgCl₂, and 10 glucose (saturated with 95% O₂ and 5% CO₂) for at least 1 h before recording. A MultiClamp 700A amplifier and pClamp 10 software (Molecular Devices, San Jose, CA, USA) were used, digitized at 2–10 kHz, filtered at 2 kHz. For neuronal whole-cell and extracellular field potential recording, slices were kept at 32 °C for 1 h after cutting and subsequently at room temperature before use. After transferring a slice into the recording chamber, the slice was perfused with aCSF at 30 °C again. A submerged chamber was mounted on an Olympus BX51WI microscope equipped for infrared-differential interference (IR-DIC) microscopy. The bath aCSF was perfused at a rate of 2 ml/min. Tetrodotoxin (TTX), AP-5, and NBQX were purchased from Tocris Bioscience (Bristol, UK). All other chemicals were purchased from Sigma-Aldrich.

Neuronal Recording Resting membrane potential (V_M) was monitored in “I = 0” mode or recorded in the current-clamp mode at least 3 min after break-in to the whole-cell neuronal recording. The electrode solution contained the following (in mM): 140 K-gluconate, 13.4 Na-gluconate, 0.5 CaCl₂, 1.0 MgCl₂, 5 EGTA, 10 HEPES, 3 Mg²⁺-ATP, and 0.3 Na⁺-GTP; 280–290 mOsm/l. Besides long-term potentiation (LTP), other recording protocols were repeated three times per cell and the replicated recordings were averaged in data analysis. Membrane capacitance (C_M) and whole-cell access resistance (R_a) were measured from the “Membrane test” protocol in the PClamp 9.2 program. For input resistance (R_{in}) analysis, a series of 300 ms current steps from –50 to +50 pA were injected at 10 pA increments, and the R_{in} was calculated as the slope of the linear fit of the voltage-current plot at the steady-state levels. Rheobase was analyzed by injecting a series of 10 ms depolarization pulses from resting V_M with 10 pA increments, and the rheobase is defined as the amplitude of the current pulse where the first AP is elicited. Action potential threshold is defined as the membrane potential where the speed of the current injection-induced voltage change reaches 20 mV/ms so that the first action potential can be induced at the lowest stimulation current. The relationship of firing frequency-injected currents was measured as the number of spikes over a 300-ms step duration in response to injected currents from 10 to 230 pA in 20 pA increments.

Miniature Postsynaptic Currents The miniature postsynaptic currents (mEPSCs) were recorded after neuronal firing and ionotropic GABA_A receptor currents were inhibited by 0.5 μ M TTX, and 100 μ M picrotoxin (PTX), respectively. mEPSC events were analyzed with Clampfit 10 using the template matching search with a minimum threshold set up at –6 pA. After collection of all the events, a visual inspection was followed for final inclusion or rejection of the events in the datasets.

Postsynaptic Current Recording Evoked excitatory postsynaptic currents (EPSCs) or potentials (EPSPs) were induced by stimulating Schaffer collaterals (SCs) in CA1 *stratum radiatum* through a local extracellular electrode (tungsten concentric bipolar microelectrode; World Precision Instruments, Sarasota, FL, USA) placed 180–250 μm from the soma of the recorded neurons. Somatic whole-cell recordings were obtained from visually identified CA1 pyramidal neurons. The pipette solution contains the following (in mM): 130 Cs-gluconate, 2 NaCl, 6 CsCl, 0.6 EGTA, 10 HEPES, 4 Mg^{2+} -ATP, 0.3 Na^{+} -GTP, 10 phosphocreatine, and 1 QX-314; 280–290 mOsm/l. The protocols for extracellular stimuli were programmed in Clampex 10 software (Molecular Devices) that were delivered through a Model A365 Isolator and A310 Stimulator (World Precision Instruments). The EPSCs were recorded at -70 mV holding potential in the presence of 100 μM PTX. The stimulation intensity of presynaptic fibers was first determined to identify the saturating level of EPSCs, and then the stimulation was scaled down to induce EPSCs at $\sim 80\%$ of the maximum amplitude for experimental recording. The evoked inhibitory postsynaptic currents (IPSCs) were recorded at 0 mV in the absence of PTX. Prior to experiments performed in PTX, a cut was made between CA1 and CA3 in the pyramidal cell layer to prevent the propagation of epileptiform activity. Neurons with $R_a < 25$ $\text{M}\Omega$ throughout the recording were qualified for inclusion for data analysis.

Paired-Pulse Facilitation The ratio of paired-pulse facilitation (PPR) was performed by the delivery of two identical intensity stimuli at an interval of 40 ms.

AMPA/NMDA Ratio The evoked AMPA and NMDA EPSCs were measured at -70 and $+40$ mV, respectively. The evoked NMDAR-mediated EPSCs were measured after AMPAR-mediated EPSC was fully decayed, e.g., 60 ms after the onset of stimulation. The pure NMDA-mediated currents were recorded at $+40$ mV in the presence of 10 μM NBQX in addition to PTX. The isolated NMDA-mediated currents could be further abolished by 50 μM AP-5 (data not shown).

Failure Rate Analysis To determine the failure rate in synaptic transmission, a minimal intensity of stimulation was used to induce EPSCs, presumably from a single or just a few synapses in a recorded CA1 pyramidal neuron. Data were collected and analyzed as described previously [17]. Stimulus trials that produce responses with an amplitude less than three times of the standard deviation (SD) of the noise were designated as synaptic failures. The failure rate was defined as the percentage of failures over the total number of stimulations. The noise amplitude was calculated on traces after inhibition of AMPA responses by NBQX.

Extracellular Field Recordings Field excitatory postsynaptic potentials (fEPSPs) were recorded in *stratum radiatum* of the CA1 area. Recording electrodes were filled with aCSF

plus 100 μM PTX with a final resistance of 2–5 $\text{M}\Omega$. Stimuli, 0.1 ms pulse width at 0.05 Hz, were delivered to the Schaffer collateral (SC) axon fibers to CA1 region through a tungsten concentric bipolar electrode. The intensity of presynaptic fiber stimulation was then reduced to the level where $\sim 30\%$ of the maximal amplitude of fEPSPs was induced to establish a basal level of fEPSPs. LTP was induced by tetanic stimulation of SC, i.e., two consecutive trains at 100 Hz for 1 s that was separated by 20 s. Prior to LTP induction, an averaged slope of the fEPSPs, i.e., from the range of 20–80%, over a 5-min duration was established as a baseline and considered to be 100%. The following slope changes in response to LTP stimulus were expressed as a percentage of this baseline (normalized slopes). An averaged slope of fEPSPs evoked between 36 and 40 min after LTP induction was used for statistical comparisons. Recordings with variations higher than 20% of baseline fEPSPs were discarded.

Recording of Astrocytes and Astrocyte Syncytial Isopotentiality Whole-cell patch-clamp recordings were made with K^{+} -based electrode solution. Astrocytes in CA1 *stratum radiatum* were identified by their small cell bodies and the linear I - V current profile [18, 19]. In the voltage-clamp recording, only those recordings with a $R_{in} < 15$ $\text{M}\Omega$ were included for data analysis. The Na^{+} -based and Cs^{+} -based electrode solutions were made by equimolar substitution of K-gluconate with Na-gluconate and Cs-gluconate, respectively. The pH was adjusted to 7.25–7.27 with KOH, NaOH, or CsOH. Rectification index (RI) was calculated by dividing the current amplitudes induced by $+20$ mV (y_1) over -180 mV (y_2) (Fig. 7d).

Immunohistochemistry

Hippocampal slices were fixed in 4% paraformaldehyde for 1 h at room temperature. The slices were blocked with 5% normal donkey serum (DNS; Jackson ImmunoResearch Laboratories, West Grove, PA, USA) and 0.01% Triton X-100 in PBS for 2 h. The primary antibodies were diluted into a 10% DNS/0.005% Triton X-100 solution and applied to slices at 4 $^{\circ}\text{C}$ overnight. They were rabbit anti-TREK-1 (1:1000, Alomone Labs, Jerusalem, Israel) and mouse anti-NeuN (1:1000; Abcam, Cambridge, MA, USA). The secondary antibodies were Cy3 donkey anti-rabbit (1:1000) and DyLight 405 donkey anti-mouse (1:1000) (Jackson ImmunoResearch Laboratories). Immunofluorescence images were obtained from a confocal microscope (TCS-SL, Leica Microsystems, Buffalo Grove, IL, USA).

Morphological Analysis of Neuronal Dendrites and Dendritic Spines

For morphological analysis of neuronal dendrites and spines, biocytin was included in K^{+} -based electrode solution (0.5 mg/ml)

for the recording of CA1 pyramidal neurons. The biocytin dialysis lasted for 15 min, and the recorded slices were then fixed with 4% paraformaldehyde for 1 h. This was followed by incubation of slices with Alexa Fluor 488 streptavidin (1:1000; Jackson ImmunoResearch Laboratories) for 4 h. The fluorescent image of neuronal dendrites and dendritic spines were acquired with $\times 20$ and $\times 63$ lens on a TCS-SL confocal microscope (Leica Microsystems). Z-series of 15 to 20 images of dendrites were compressed into two dimensions using the maximum projection of the Leica software. Dendritic complexity was assessed with the Sholl analysis in ImageJ software [20], including analysis of total dendritic length and number of branch points. The number of spines was manually counted in tertiary branches of CA1 pyramidal neurons. Spines were counted only if they had both a punctuate head and visible neck. Spines were subclassified into mushroom, stubby, thin, and filopodia according to a previous report [21].

Immunoblotting

Hippocampi from wild-type and TREK-1 KO mice were homogenized in RIPA lysis buffer with protease inhibitor mixture. Equal amounts of protein (25 $\mu\text{g}/\text{well}$) were separated on a 10% SDS-PAGE gel followed by transfer to nitrocellulose membranes. After blocked with 5% non-fat milk, the membranes were probed with primary antibodies: rabbit anti-PSD95 (1:1000, Abcam), mouse anti-synaptophysin (SY38) (1:1000, Abcam), or rabbit anti-GAPDH (1:8000, Sigma-Aldrich) at 4 °C overnight. After secondary antibody incubation (1:100,000, Goat Anti-Rabbit and Goat Anti-Mouse, Jackson ImmunoResearch Laboratories), immunoreactivity was detected with an enhanced chemiluminescent detection (Thermo Fisher Scientific, Rockford, IL, USA). All the three proteins were detected from the same membrane by using stripping buffer to strip off the first primary antibody and re-probing with the second one. GAPDH was used as a loading control. Blots were scanned and quantified by ImageJ software. The expression level of synaptophysin and PSD95 was normalized to that of GAPDH.

Novel Object Recognition

Novel object recognition (NOR) is a behavioral test for learning and memory, in particular, recognition memory [10]. Following the protocol described in a previous study [22], this test was performed in an open field (45 \times 45 \times 40 cm, Panlab, Spain). First, the mice were individually habituated to the open field by freely exploring for 5 min. After 24 h, the mice were placed back into the same arena to be familiarized with two identical objects for 10 min. After 6 h post-familiarization, one of the familiar objects was replaced by a novel object different in its shape, color, and texture and mice were left to explore both objects. The objects employed in the NOR test were towers of Lego bricks (8 cm high and 3.2 cm wide, built in blue, yellow, red,

and green bricks) and Falcon tissue culture flasks filled with sand. A minimal exploration time of 20 s for both objects during the test phase was used. The position of the novel object and the associations of the novel and familiar were randomized. This session was videotaped and the time subjects spent interacting with each object was recorded manually. Object exploration was defined as the orientation of the nose to the object at a distance of less than 2 cm. Memory performance was assessed by the discrimination index (DI), as defined by (novel object exploration time/total exploration time) \times 100. A higher discrimination index is considered to reflect greater memory retention for the familiar object. Prior to testing, we have profiled TREK-1 KO mice for gross deficiencies in sensory perception and locomotor activity to rule out their potential influence on the performance in the chosen behavioral tests. Overall, no obvious developmental abnormalities, or deficits in locomotor activity, touch, vision, or hearing, were evident in TREK-1 KO mice.

Data Analyses

The patch-clamp recording data were analyzed by Clampfit 9.0 (Molecular Devices) and Origin 8.0 (OriginLab, Northampton, MA, USA). After evaluating data for normality and homoscedasticity, statistical analysis was performed using Student's *t* test or a two-way ANOVA followed by a post hoc Tukey HSD test. The Mann–Whitney nonparametric test was chosen when data were not normally distributed. The Kolmogorov–Smirnov test was used to test the cumulative probability of mEPSCs median amplitudes and mean frequencies. Group data are presented as mean \pm SEM, and *n* is the number of brain slices, unless otherwise stated. In a given brain slice, the patch recording was performed in only one neuron. The tests were two-sided and significance was set at $P < 0.05$; *, **, and *** refer to *P* values lower than 0.05, 0.01, and 0.001, respectively.

Results

Genetic TREK-1 Deletion Depolarizes Membrane Potential of Pyramidal Neurons

We found that TREK-1 staining was well co-localized with neuronal marker NeuN on CA1 pyramidal neurons in acute hippocampal slices (Fig. 1a). To determine the contribution of TREK-1 to neuronal membrane potential (V_M), whole-cell patch recording was performed. TREK-1 KO significantly depolarized the resting V_M of CA1 pyramidal neurons compared to WT neurons (WT, -66.9 ± 0.4 mV, $n = 26$ vs. TREK-1 KO, -62.9 ± 0.4 mV, $n = 29$; $P < 0.001$; Fig. 1b). The contribution of TREK-1 as a leak K^+ channel to resting V_M was also indicated by a higher membrane input resistance (R_{in}) in TREK-1 KO (162.8 ± 11.9 M Ω , $n = 18$) than WT ($126.5 \pm$

8.6 M Ω , $n = 18$; $P = 0.019$) (Fig. 1c). To corroborate this finding, the neurons were then recorded with a Cs⁺-based electrode solution for the elimination of the entire K⁺ conductance [23]. This resulted in an overall increase in neuronal R_{in} and abolished the difference between WT and TREK-1 KO CA1 pyramidal neurons (TREK-1 KO, 274.2 \pm 21.8 M Ω , $n = 28$ vs. WT, 243.7 \pm 20.9 M Ω , $n = 22$; $P = 0.327$; Fig. 1c). These together support the view that TREK-1 is a highly expressed and important background K⁺ channel for the setting of neuronal resting V_M .

The membrane capacitance (C_M) did not differ between TREK-1 KO and WT neurons in recordings made with K⁺- or Cs⁺-based electrode solutions (Fig. 1d), indicating that TREK-1 KO does not have a detectable change in neuronal surface area (but see the difference in the following dendritic sprouting and spine density analysis in Fig. 3e–g).

TREK-1 KO Enhances the Excitability of Pyramidal Neurons

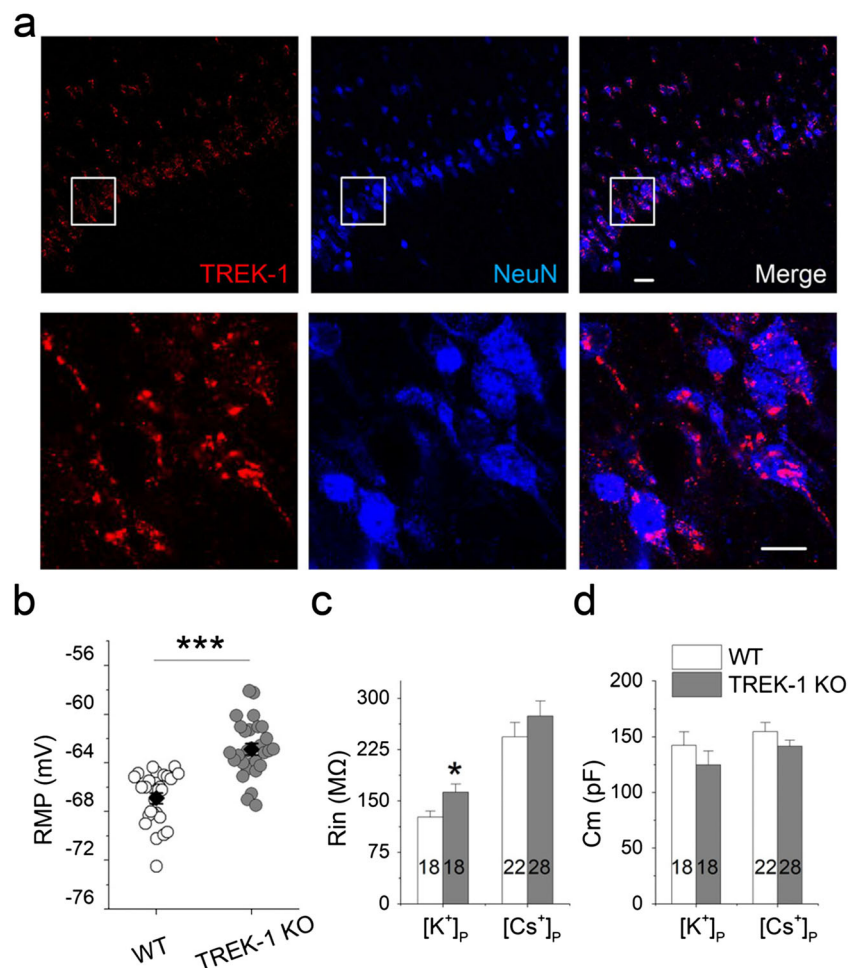
A more depolarized V_M in TREK-1 KO neurons implies a higher sensitivity to afferent presynaptic inputs for generating

action potentials (Fig. 1b). Indeed, somatic current injection induced a higher action potential (AP) firing rate in TREK-1 KO pyramidal neurons than WT (Fig. 2a). Consistently, the rheobase currents, i.e., the minimum positive currents for induction of action potential, were 30% less in TREK-1 KO pyramidal neurons than WT (TREK-1 KO, 49.4 \pm 6.4 pA, $n = 16$ vs. WT, 72.3 \pm 7.7 pA, $n = 11$; $P = 0.031$; Fig. 2b, c). Also, TREK-1 KO shifted the threshold for AP significantly towards a depolarized value (TREK-1 KO, -41.5 \pm 1.1 mV, $n = 21$ vs. WT, -45.5 \pm 1.4 mV, $n = 18$; $P = 0.033$; Fig. 2b, d). TREK-1 KO, however, did not alter the amplitude of the evoked action potentials (Fig. 2e).

TREK-1 KO Increases Dendritic Sprouting and Spine Density

Spadin, a TREK-1 inhibitor as well as an antidepressant, was shown to facilitate the maturation of dendritic spines in cortical neurons [24]. Thus, we next examined the impact of TREK-1 deficiency on neuronal dendritic sprouting and spines. The CA1 pyramidal neurons were first filled with biocytin during recording, and that was followed by neuronal morphological analysis.

Fig. 1 TREK-1 KO depolarizes membrane potential and increases input resistance of hippocampal pyramidal neurons. **a** TREK-1 (left) and neuronal marker NeuN (middle) immunostaining in the hippocampal CA1 region. Areas outlined in the square boxes are shown in higher magnification in the lower panels where TREK-1 and NeuN staining are nicely colocalized in neuronal soma and primary dendritic processes. Scale bar represents 25 μ m. **b** TREK-1 KO depolarizes the resting membrane potential of CA1 pyramidal neurons. **c** TREK-1 KO increases the input resistance (R_{in}) of CA1 pyramidal neurons in K⁺-based physiological pipette solution ([K⁺]_p) but not in Cs⁺-based pipette solution ([Cs⁺]_p). **d** The membrane capacitance (C_M) is not altered in CA1 pyramidal neurons in TREK-1 KO mice. Numbers of neurons analyzed are shown in bars. Statistical significance was evaluated by Student's *t* test. (* $P < 0.05$; *** $P < 0.001$)



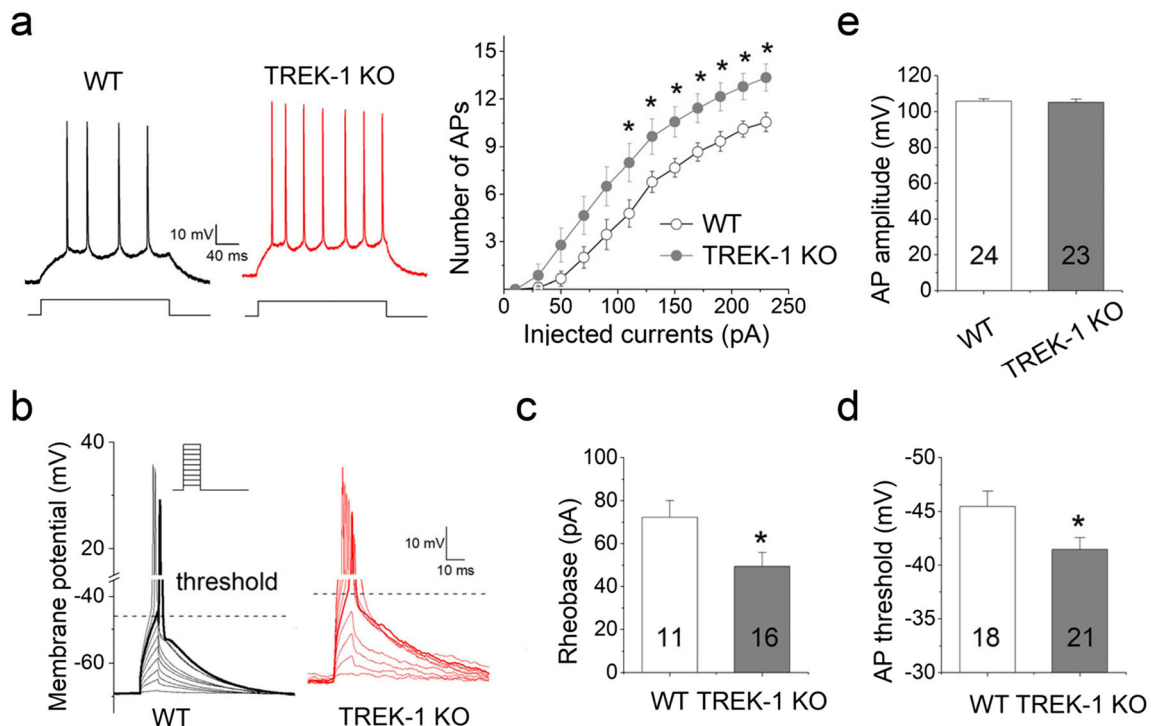


Fig. 2 TREK-1 KO increases the excitability of CA1 pyramidal neurons. **a** Left, a 100 pA/300 ms current step induced 4 and 7 spikes in a WT and TREK-1 KO CA1 pyramidal neuron, respectively. Cells were held at -70 mV. Right, a series of current steps, ranging from 10 to 230 pA at 300 ms duration and 20 pA increment, induced a steeper current input-spike output relationship in TREK-1 KO ($n = 14$) than WT neurons ($n = 9$). **b** Rheobase current for neuronal firing threshold. The inset shows the current steps from 10 to 100 pA steps at 10 ms duration and 10 pA

increments for detecting of the rheobase current and threshold (dash line) for neuronal firing in a WT and TREK-1 KO neuron, respectively. **c** TREK-1 KO significantly reduces the rheobase currents. **d** TREK-1 KO decreases the threshold for neuronal firing. **e** TREK-1 KO does not affect the amplitude of neuronal firing spikes. Statistical significance was evaluated by Student's *t* test (bar graphs) or two-way ANOVA followed by a post-hoc Tukey HSD test (input-output plots). * $P < 0.05$

TREK-1 KO did not alter the overall neuronal morphology in terms of the total dendritic length (Fig. 3a, b). However, in Sholl analysis, the branching of apical dendrites increased significantly in TREK-1 KO pyramidal neurons (TREK-1 KO, 25.7 ± 2.2 , $n = 10$ neurons vs. WT, 19 ± 1.6 , $n = 11$ neurons; $P = 0.021$; Fig. 3c); there were more dendritic branching intersections located 70–155 μm distal from the somatic center (Fig. 3d). These results indicate that TREK-1 deficiency alters the branching pattern of CA1 pyramidal neurons.

Variation of the spine shapes and density occurs in different stages of neuronal dendritic and functional circuit maturation [21]. TREK-1 KO significantly increased the spine density of CA1 pyramidal neurons (TREK-1 KO, 9.0 ± 0.4 spines/10 μm , $n = 23$ dendritic segments/8 neurons/4 mice; WT, $n = 8.0 \pm 0.3$ spines/10 μm , $n = 19$ dendritic segments/8 neurons/7 mice; $P = 0.027$, Fig. 3e, f). Further analysis showed that the density of mature spines, i.e., mushroom and stubby, did not differ between TREK-1 KO and WT (TREK-1 KO, 5.5 ± 0.3 spines/10 μm , $n = 23$ dendritic segments/8 neurons/4 mice; WT, 5.6 ± 0.2 spines/10 μm , $n = 19$ dendritic segments/8 neurons/7 mice; $P = 0.752$). However, the immature spines, i.e., the thin and filopodia, showed a significant increase in TREK-1 KO neurons (TREK-1 KO, 3.6 ± 0.3 spines/10 μm , $n = 23$ dendritic segments/8

neurons/4 mice; WT, 2.4 ± 0.2 spines/10 μm , $n = 19$ dendritic segments/8 neurons/7 mice; $P = 0.001$) (Fig. 3e–g).

To answer whether a higher amount of immature spines in TREK-1 KO could correlate to a higher amount of synapses, western blot was carried out to compare the pre- and postsynaptic proteins synaptophysin and PSD-95 (Fig. 3h). Nevertheless, neither synaptophysin nor PSD-95 expression differed between WT and TREK-1 KO mice. Specifically, synaptophysin expression (normalized to GAPDH) was 0.83 ± 0.08 for WT ($n = 4$) and 0.88 ± 0.09 for TREK-1 KO ($n = 4$), and the PSD-95 expression was 0.87 ± 0.09 for WT ($n = 4$) and 0.79 ± 0.11 for TREK-1 KO ($n = 4$), respectively.

Together, these results indicate that TREK-1 deficiency alters neuronal dendritic branching and increases the density of immature spines in CA1 pyramidal neurons.

TREK-1 KO Increases Both Excitatory and Inhibitory Synaptic Transmission onto CA1 Pyramidal Neurons

To determine whether a deficiency in TREK-1 affects the strength of CA3 SC-CA1 synaptic transmission, we first examined the mEPSCs in CA1 pyramidal neurons (see “Materials and methods”). In the presence of TTX and PTX

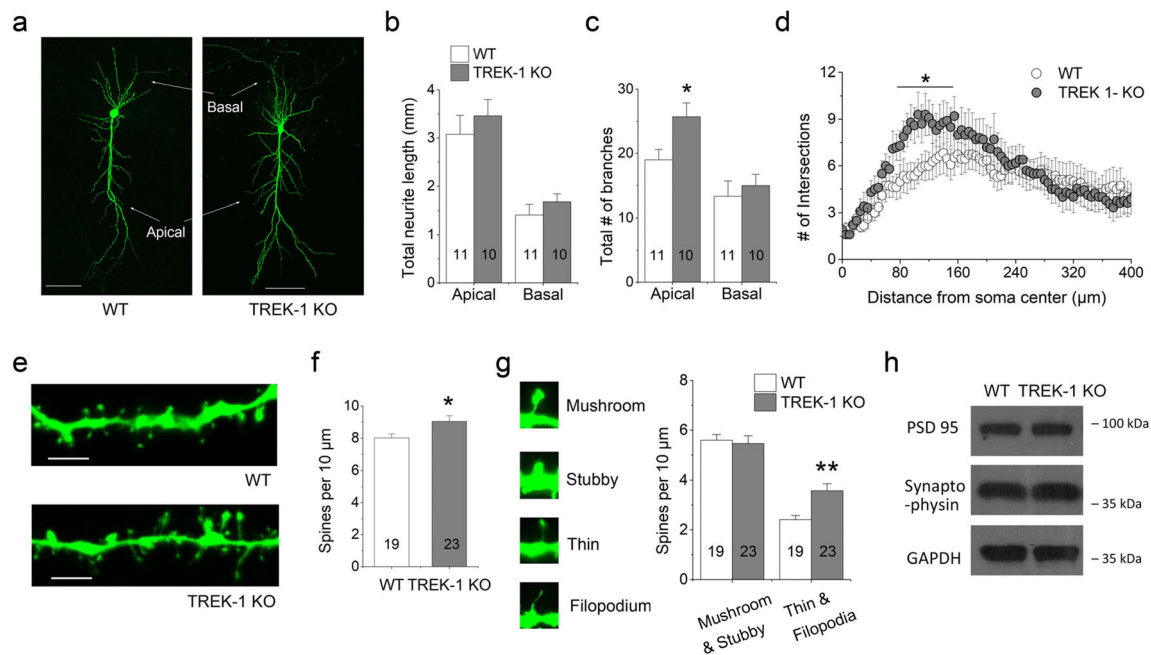


Fig. 3 TREK-1 null alters dendritic sprouting and the number of spines. **a** Representative images of CA1 pyramidal neurons revealed by electrode biocytin-loading followed by Alexa 488-conjugated streptavidin staining. Scale bar, 100 μm . **b–d** Summary of the total dendritic length (**b**), branch numbers (**c**) in both apical and basal dendritic trees, and apical dendritic arborization in terms of the number of intersections (**d**). **e** Representative higher resolution 3D confocal dendritic segment images for spine detection, classification, and measurements. Scale bar, 3 μm . **f** Summary of the dendritic spine densities in WT and TREK-1 KO groups. **g** Quantification of dendritic spine subtypes. *Left*, images of the four different spine

subtypes. *Right*, quantification of mature and immature dendritic spine subtypes of CA1 neurons. The numbers of the dendritic segments used for quantification are shown in the bars, and these segments were obtained from 4 to 7 mice in each group. **h** Western immunoblots show comparable levels of expression of presynaptic (synaptophysin), and postsynaptic (PSD-95) proteins in WT and TREK-1 KO mice. GAPDH was used as a protein quantity loading control. Data for all bar graphs were analyzed using Student's *t* test. In **c**, the comparison of the number of intersections between the two groups was analyzed using repeated-measures two-way ANOVA. (* $P < 0.05$; ** $P < 0.01$)

for inhibition of neuronal firing and inhibitory synaptic transmission, the frequency of mEPSCs was 47% higher in TREK-1 KO neurons than that of the WT (TREK-1 KO, 0.69 ± 0.06 Hz, $n = 10$ vs. WT, 0.47 ± 0.08 Hz, $n = 9$; $P = 0.034$; Fig. 4a), and this is associated with a left-shifted cumulative probability curve of inter-event intervals in TREK-1 KO neurons (K-S test, $z = 1.99$; $P < 0.001$). Meanwhile, the cumulative probability curve of mEPSCs amplitudes was not altered in TREK-1 KO neurons (Fig. 4a right). This indicates that TREK-1 KO increases the probability, but may not affect the quantal size, of presynaptic glutamate release in SC-CA1 synapses.

In the second study, the evoked AMPA receptor-mediated excitatory postsynaptic currents (AMPA-EPSCs) in CA1 pyramidal neurons were recorded upon stimulation of SC with incremental voltage steps. In response to SC stimulation, the amplitude of AMPA-EPSC was increased by 25.8% at 0.35 mA, 25.4% at 0.4 mA, 24.3% at 0.45 mA, and 22.8% at 0.5 mA in TREK-1 KO ($n = 19$) relative to WT neurons ($n = 17$, $P < 0.05$, Fig. 4b right).

In the third study, the SC stimulation evoked AMPA-EPSCs, and GABA_A receptor-mediated IPSCs were examined from the same neurons by holding the V_M at -70 and 0 mV, respectively (Fig. 4c). The results show that TREK-1 KO

increases the amplitude of both EPSCs (TREK-1 KO, -577 ± 59 pA, $n = 17$ vs. WT, -414 ± 38 pA, $n = 17$; $P = 0.028$) and IPSCs (TREK-1 KO, 628 ± 58 pA, $n = 17$ vs. WT, 466 ± 42 pA, $n = 17$; $P = 0.03$; Fig. 4c). Thus, there is a general augmentation in synaptic transmission in TREK-1-deficient neurons.

TREK-1 KO Increases Functional Expression of Postsynaptic AMPA Receptors

Elevated functional expression of postsynaptic AMPA receptors could contribute to the observed increase of EPSCs in TREK-1-deficient neurons. To explore this possibility, we examined the ratio of AMPA-EPSCs over NMDA receptor-mediated EPSCs (NMDA-EPSCs). The AMPA-EPSCs and NMDA-EPSCs in the same neurons were sequentially evoked by SC stimulation at the holding voltages of -70 and $+40$ mV, respectively (Fig. 5a). A 35% increase in the AMPA-EPSC/NMDA-EPSC ratio was evident in TREK-1 KO pyramidal neurons (ratio of TREK-1 KO, 2.27 ± 0.44 , $n = 8$; WT, 1.70 ± 0.44 , $n = 8$; $P = 0.015$; Fig. 5a). To further substantiate this notion, the pure NMDA-EPSCs were isolated in the presence of NBQX and PTX for inhibition of AMPA-EPSCs and

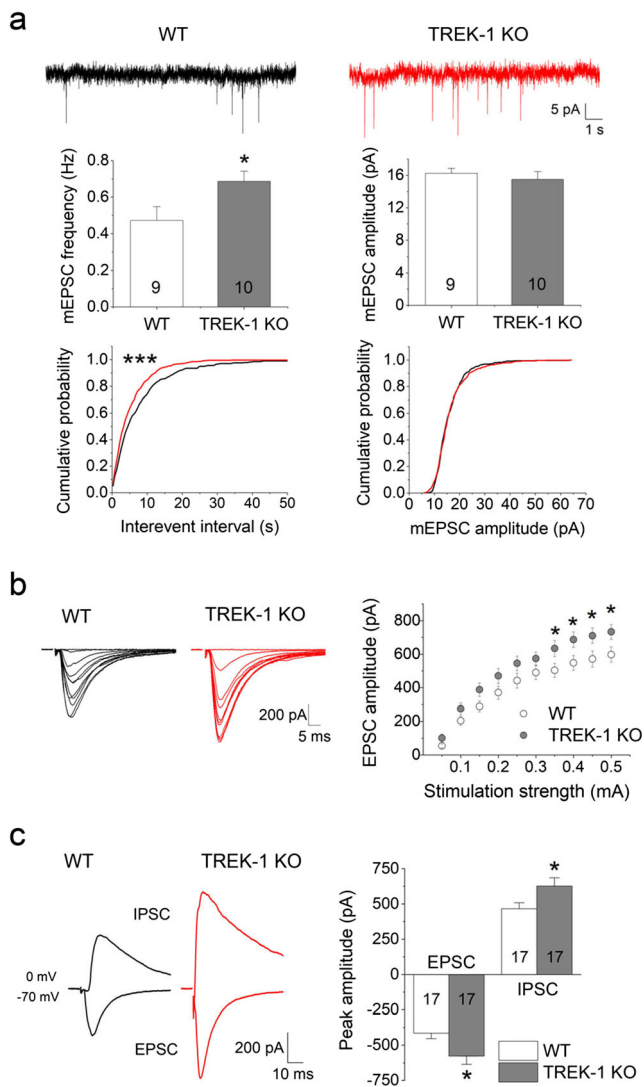


Fig. 4 TREK-1 KO increases excitatory and inhibitory synaptic transmission in CA1 pyramidal neurons. **a** The frequency but not the amplitude of mEPSCs increases in TREK-1 KO neurons. mEPSCs were recorded in the presence of 0.5 μ M TTX and 100 μ M PTX. *Top*, representative mEPSCs traces; *bottom*, the cumulative probability of the mEPSC frequency (left) and amplitude (right). **b** Input-output relationship of EPSCs in CA1 neurons. Input refers to graded electrical stimulation of Schaffer collateral (SC), whereas output refers to SC stimulation-induced whole-cell EPSCs. The neuronal EPSCs outputs show an increase in TREK-1 KO neurons ($n = 19$) compared to wild-type neurons ($n = 17$). **c** *Left*, the SC stimulation-induced EPSCs and IPSCs were recorded from the same neuron by varying holding V_M from -70 to 0 mV, respectively. TREK-1 KO resulted in an enhanced EPSCs and IPSCs compared to wildtype ($P < 0.05$). *Right*, a summary of the data. Statistical significance was evaluated by Student's t test (bar graphs), Kolmogorov-Smirnov test (cumulative probability plots), or two-way ANOVA followed by a post-hoc Tukey HSD test (input-output plot). * $P < 0.05$; *** $P < 0.001$

IPSCs, respectively. The amplitude of pure NMDA-EPSC, however, did not differ between TREK-1 KO and WT neurons (TREK-1 KO, 227 ± 52 pA, $n = 8$; WT, 214 ± 56 , $n = 6$; $P = 0.875$; Fig. 5b). Thus, increased expression of functional AMPA receptor currents indeed contributes as an additional

mechanism to the enhanced excitatory synaptic transmission in TREK-1 KO CA1 pyramidal neurons.

TREK-1 KO Increases the Ratio of Active/Silent SC-CA1 Synapses on Pyramidal Neurons

Postsynaptic trafficking of AMPAR plays an important role in synaptic plasticity [25]. Additionally, a decrease in the ratio of AMPA receptor-lacking (silent) over AMPA receptor-expressing (active) synapses has been shown to underlie the expression of LTP in hippocampal CA1 region [26]. Thus, we asked whether elevated expression of postsynaptic AMPA-EPSCs would correspond to a higher ratio of active synapses in TREK-1-deficient neurons. We explored this by analyzing the failure rate of synaptic AMPA-EPSCs and NMDA-EPSCs that were induced by a minimum electrical stimulation delivered onto SC (see “Materials and methods”) [17].

We show that the failure rate of AMPA-EPSCs in response to minimum SC stimulations was lower in TREK-1 KO neurons (failure rate: TREK-1 KO, $37.7 \pm 3.9\%$, $n = 9$ vs. WT, $49.5 \pm 3.9\%$, $n = 10$, $P = 0.046$). Additionally, the amplitude of AMPA-EPSCs was higher in TREK-1 KO neurons (AMPA-EPSCs: TREK-1 KO, -21.9 ± 0.9 pA, $n = 9$ vs. WT, -17.9 ± 1.0 pA, $n = 10$; $P = 0.008$) (Fig. 5c–e). In contrast, the NMDA-EPSCs induced at the holding potential of $+40$ mV did not differ between the two groups, suggesting that the overall quantity of glutamatergic synapses remains unchanged in TREK-1 KO neurons (Fig. 5f). Thus, TREK-1 KO increases the ratio of AMPA-expressing active synapses in CA1 pyramidal neurons.

TREK-1 Deficiency Occludes Long-Term Potentiation and Impairs Recognition Memory

Profound deficits in CA1 pyramidal neuron structure, excitability, and synaptic transmission promoted us to further examine the holistic impact of these anatomic and functional changes on the plasticity of synaptic plasticity and memory formation in the following studies.

The paired-pulse ratio (PPR) was carried out to determine if the high probability of presynaptic glutamate release has an impact on short-term plasticity. We found that the PPR was indeed depressed in TREK-1 KO neurons (TREK-1 KO, 1.69 ± 0.06 , $n = 17$ vs. WT, 1.86 ± 0.05 , $n = 16$; $P = 0.044$; Fig. 6a). This is consistent with the enhanced presynaptic release in basal neurotransmission (Fig. 4a) as well as EPSCs in TREK-1-deficient neurons (Fig. 4b).

In the following study, tetanus stimulation paradigm was used to induce LTP in the CA1 region (see “Materials and methods” for details). We showed that TREK-1 deficiency occluded LTP by 30% (36–40 min after tetanus stimulation, $n = 10$) compared with WT mice ($n = 12$; $P = 0.008$; Fig. 6b, c).

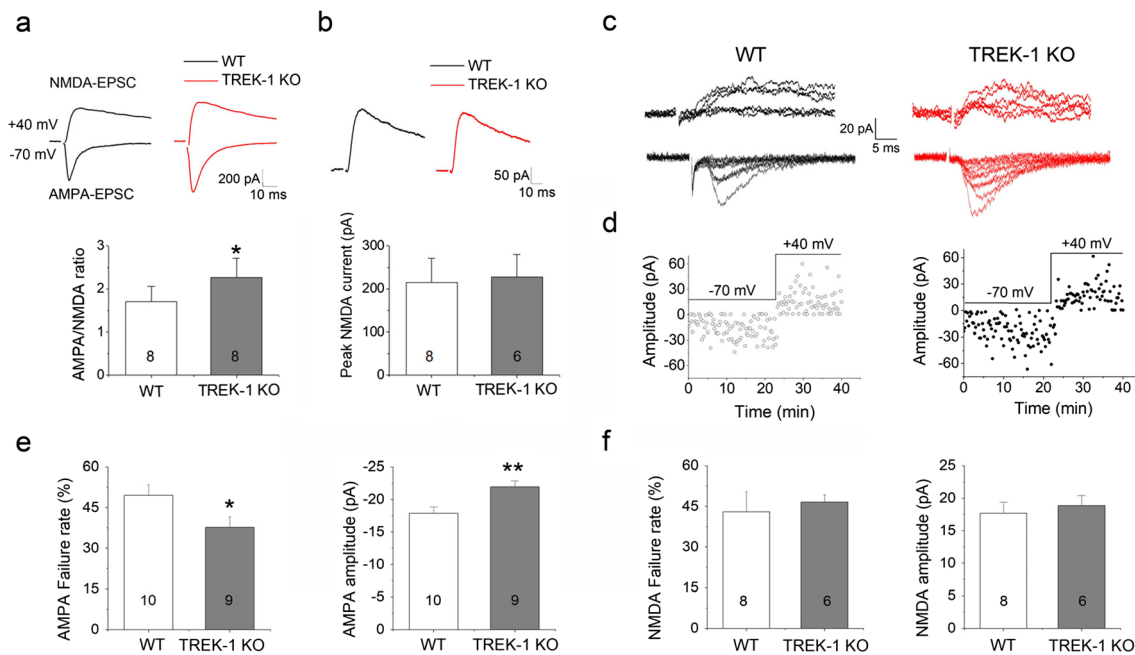


Fig. 5 TREK-1 KO increases the active/silent ratio of SC-CA1 glutamatergic synapses. **a** In the presence of PTX, the AMPA-EPSC and NMDA-EPSC in CA1 pyramidal neurons were induced by SC stimulation at the holding V_M of -70 and $+40$ mV, respectively. TREK-1 KO increases the AMPA-EPSC/NMDA-EPSC ratio. **b** The amplitudes of SC stimulation-induced NMDA receptor currents are comparable between WT and TREK-1 KO neurons. The NMDA receptor currents were isolated by adding PTX and NBQX for inhibition of $GABA_A$ and AMPA receptors, respectively. **c** Minimal SC stimulation-induced AMPA-EPSC (holding at -70 mV) and NMDA-EPSC (holding at $+40$ mV) in WT and TREK-1 KO neurons. In each case, 6 consecutive traces are superimposed to show the variation from absence to the presence of SC

stimulation-induced EPSCs. The NMDA-EPSCs were recorded in the presence of $10 \mu\text{M}$ NBQX. **d** Use of minimal SC stimulation, the induced and failed EPSC events are plotted over a 40-min duration in a WT and TREK-1 KO neuron as indicated. In each case, the AMPA-EPSC events were recorded first by holding the cell at -70 mV, and the NMDA-EPSC events were recorded afterward by switching the holding to $+40$ mV in the presence of $10 \mu\text{M}$ NBQX. **e** Summary of the data from **d**, a less failure rate without affecting the amplitude of minimal SC stimulation-induced AMPA-EPSCs occurred in TREK-1 KO neurons. **f** Summary of the data from **d**, no change in either the failure rate or the amplitude of minimal SC stimulation-induced NMDA-EPSCs in TREK-1 KO neurons. Student's *t* test was used. * $P < 0.05$; ** $P < 0.01$

To further establish the physiological consequence of TREK-1 KO on memory, we tested the novel object recognition memory task (NOR) between TREK-1 KO and WT mice. Only one out of the 22 tested mice in our sample data set did not reach the criterion. The TREK-1 KO mice displayed a significant decrease in discrimination index, indicative of a memory deficit (TREK-1 KO, $51.9 \pm 2.7\%$, $n = 11$ vs. WT, $65.5 \pm 3.1\%$, $n = 10$, $P = 0.003$; Fig. 6d). There was no alteration in total object exploration time.

Altogether, these findings indicate that deficiency in TREK-1 impairs the plasticity of glutamatergic synaptic transmission and novel object recognition memory.

TREK-1 KO Does Not Alter Astrocyte K^+ Conductance and Astrocyte Syncytial Function

A high-density expression of leak K^+ conductance is a characteristic of astrocytes that is critical for glutamate and K^+ clearance during neuronal activities [27]. Thus, the enhanced basal synaptic transmission in the TREK-1 KO hippocampus may be at least in part due to the impaired TREK-1 function in astrocytes for homeostatic regulation of extracellular

environment and neurotransmitters, such as glutamate and GABA. Although the astrocytic expression of TREK-1 is evident, its impact on astrocyte K^+ conductance could not be confirmed in our early reports [15, 16].

To further examine the role of TREK-1 in astrocytes, we first examined the astrocytic expression of TREK-1 by immunocytochemistry. TREK-1 immunoreactivity, however, was mainly detected from NeuN-positive CA1 pyramidal neurons, but not Aldh111-eGFP-positive astrocytes (Fig. 7a). This is consistent with our previous observations where TWIK-1 and $K_{ir}4.1$ were the major K^+ channels in hippocampal astrocytes [15, 16].

We then electrophysiologically recorded astrocytes from the hippocampal CA1 region. There was no difference in resting V_M between TREK-1 KO and WT astrocytes (TREK-1 KO, -74.6 ± 0.3 mV, $n = 31$ vs. WT, -75.2 ± 0.4 mV, $n = 33$, $P = 0.2$; Fig. 7b). Also, TREK-1 KO did not alter the linear current-to-voltage (*I-V*) relationship (Fig. 7c), suggesting a negligible contribution of TREK-1 to the overall astrocyte passive K^+ conductance. In addition, if the outwardly rectifying TREK-1 contributes substantially to membrane passive conductance, TREK-1 KO would increase the inward rectification of whole-cell current with a reduced RI value.

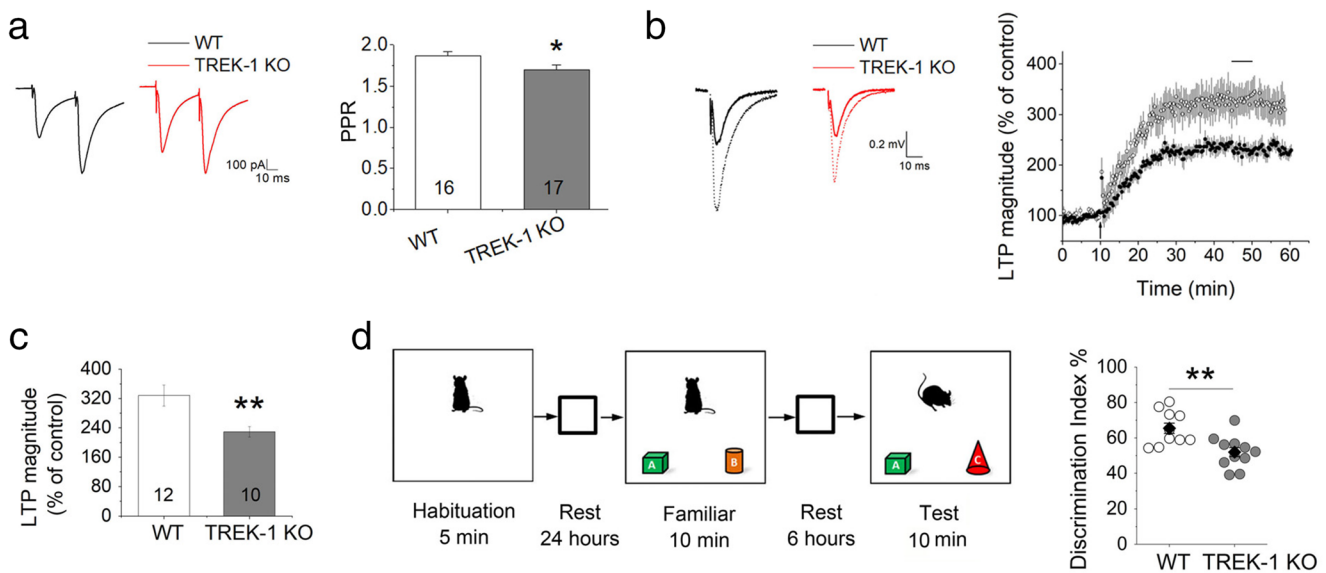


Fig. 6 TREK-1 KO depresses the ratio of paired-pulse facilitation, occludes long-term potentiation, and impairs hippocampal-dependent space memory. **a** TREK-1 KO decreases the ratio of paired-pulse facilitation (PPR) of CA3–CA1 synapses. *Left*, in a WT and TREK-1 KO neuron as indicated, two consecutive EPSCs were induced by SC stimulation pulses at 40 ms interval. **b** LTP in the CA1 region was induced by high-frequency stimulation of SC (HFS, arrow). The LTP in TREK-1 KO mice was markedly occluded ($n = 10$) when compared to WT ($n = 12$). *Left*, representative fEPSP traces CA1 region before (solid traces) and 40 min

after HFS of SC afferents (dashed traces) in WT and TREK-1 KO mice. **c** Quantification of fEPSP slope change reveals a TREK-1 KO-induced occlusion of LTP. The quantification was made by averaging normalized fEPSP slope from 36 to 40 min after HFS, as a short line indicated in the time course of **b**. **d** New object recognition. *Left*, schematic for test protocol. *Right*, the summary graph shows TREK-1 KO mice ($n = 11$) spent less time on new objects than WT mice ($n = 10$), as the discrimination index decreasing. Student's *t* test was used. * $P < 0.05$; ** $P < 0.01$

However, the RI was essentially unchanged in TREK-1 KO astrocytes (TREK-1 KO, 0.94 ± 0.02 , $n = 6$ vs. WT, 0.91 ± 0.01 , $n = 6$; $P = 0.197$, Fig. 7d). Together, consistent with our previous report [15], the basic electrophysiological features remain intact in TREK-1 KO astrocytes.

Astrocytes are strongly electrically coupled through gap junctions to achieve a state of syncytial isopotentiality, and this network mechanism has been demonstrated to be crucial for the regulation of extracellular K^+ concentration [28]. To determine whether TREK-1 KO disrupts syncytial isopotentiality, we equimolarly substituted the physiological K^+ ion with Na^+ or Cs^+ in pipette solution ($[Na^+]_p$, $[Cs^+]_p$) for whole-cell astrocyte recording. $[Na^+]_p$ or $[Cs^+]_p$ is anticipated to depolarize the recorded astrocyte to 0 mV following the prediction by the Nernst equation [28]. In a syncytial coupled astrocyte, this $[Na^+]_p$ - or $[Cs^+]_p$ -induced depolarization can be compensated to a quasi-physiological level by the neighboring astrocytes due to gap junctional coupling (Fig. 7e) [28, 29]. In TREK-1 KO mice, the steady-state astrocyte V_M ($V_{M,ss}$) remained at quasi-physiological levels in recordings made with $[Na^+]_p$ and $[Cs^+]_p$ that was comparable to the physiological V_M recorded with $[K^+]_p$. And we did not observe any differences in $V_{M,ss}$ between WT and TREK-1 KO astrocytic networks (Fig. 7e), indicating that TREK-1 KO does not alter the function of astrocyte syncytium. Together, TREK-1 deficiency does not alter astrocyte membrane K^+ conductance or syncytial network function.

Discussion

In the present study, we show that genetic deletion of TREK-1 results in alterations of neuronal dendritic sprouting and spines, heightening of neuronal excitability, and disruption of synaptic transmission and plasticity. These anatomic and functional changes are associated with impaired hippocampal memory. Thus, TREK-1 appears to be a critical player in basic neuronal physiology and brain cognitive function.

TREK-1 Deficiency Alters the Neuronal Structure

In TREK-1 KO mice, we observed an increase of neuronal dendritic sprouting and spines. Although the gross length of the dendrites remains unchanged, TREK-1 KO increases the branch sprouting and spine density in CA1 pyramidal neurons (Fig. 3b–d). This observation adds to a growing list of evidence in which K^+ channels have been shown to regulate dendritic maturation. For example, in retinal ganglion cells, Kv1.1 regulates the development of dendritic arborization through control of membrane excitability [30]. In somatosensory thalamocortical neurons, neuronal hyperexcitability, induced by Kv1.1 repression, impairs dendritic maturation, whereas overexpression of Kv1.1 is sufficient to restore the synaptic connectivity during postnatal development [31]. While the evidence that K^+ channels regulate dendritic sprouting and spine morphology have been mainly reported

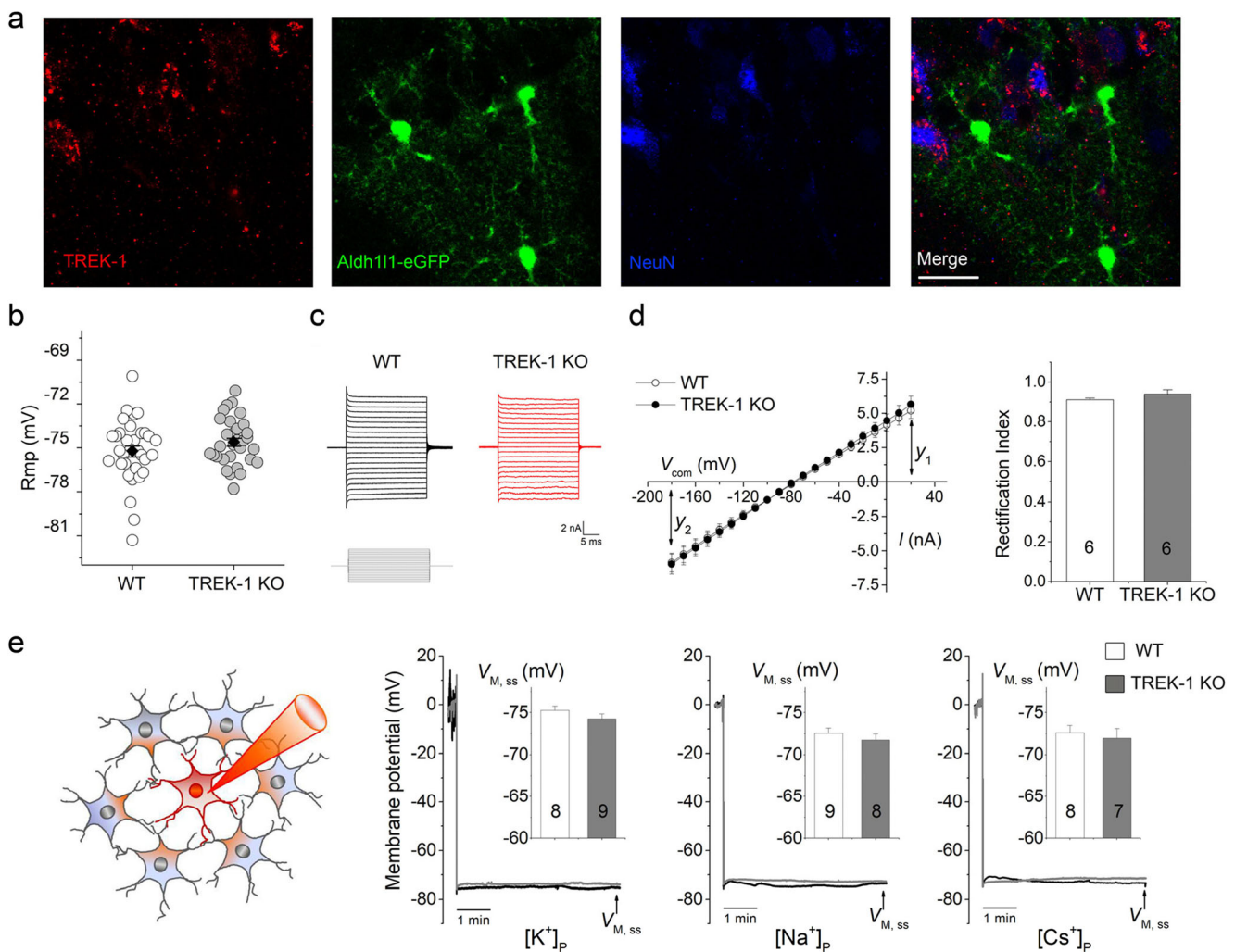


Fig. 7 TREK-1 KO does not alter astrocyte K⁺ conductance or astrocyte syncytial isotopotentiality. **a** TREK-1 immunostaining signal is negligible in astrocytes. TREK-1 (red), NeuN (blue) double staining in Aldh111-eGFP mouse in CA1 region. Scale bar, 25 μm . **b** TREK-1 OK does not alter the resting V_M of hippocampal astrocytes in CA1 region (WT, $n = 33$; TREK-1 KO, $n = 31$). **c** TREK-1 KO does not alter the passive K⁺ conductance of astrocytes. Astrocyte was held at -80 mV and the membrane currents were induced by command voltages from -180 to $+20$ mV with 10 mV increment (inset, command voltages). Astrocytes in both genotypes showed a similar linear I - V relationship membrane

conductance (passive) and comparable amplitude of passive conductance. **d** The I - V curves that were constructed from the current amplitudes. The current amplitude at y_1 (V_{+20} mV) and y_2 (V_{-180} mV) was used to calculate the rectification index (RI) (see “Materials and methods”). **e** Astrocyte syncytial isotopotentiality remains intact in TREK-1 KO mice. *Left*, a schematic illustration of the use of non-physiological $[\text{Na}^+]_p$ or $[\text{Cs}^+]_p$ to examine the existence of syncytial isotopotentiality in an astrocyte network. *Right*, representative $V_{M,ss}$ recordings with $[\text{K}^+]_p$, $[\text{Na}^+]_p$, and $[\text{Cs}^+]_p$, respectively. Insets show an unchanged $V_{M,ss}$ in TREK-1 KO astrocytes. Student’s t test was used.

from certain brain regions in the developing brain, the exact mechanisms underlying this process is still under debate [31].

Based on the structure stability–function relationship, the dendritic spines can be classified into two categories, small and large [32]. Small spines (thin and filopodia spines) are functionally immature, whereas large spines (mushrooms and stubby spines) are structurally stable to maintain strong synaptic connections. In TREK-1 KO neurons, we observed an overall increase in the density of dendritic spines. However, it is the immature spines that account for the observed increase in dendritic spines (Fig. 3g). Considering that immature spines contain a low level of PSD-95, an increase in the number of immature spines on the dendrites should contribute insignificantly to the total amount of

PSD-95. Indeed, the quantity of two critical synaptic proteins synaptophysin and PSD-95 was not altered by TREK-1 KO (Fig. 3h), which favors the view that TREK-1 KO does not alter the totality of functional synapses.

In a previous study, pharmacological inhibition of TREK-1 by spadin increased the proportion of mature spines without affecting spine densities in cultured cortical neurons [24]. The difference between this observation and our finding is likely due to the varied approaches that were used for TREK-1 manipulation; the genetic knockout was used in our study, whereas in the study reported by others, spadin was used to pharmacologically inhibit TREK-1 in cultured cortical neurons.

TREK-1 Deficiency Increases Neuronal Excitability

As a leak type K^+ channel, genetic TREK-1 knockout produced an anticipated neuronal membrane potential (V_M) depolarization and increase in membrane resistance (R_M) (Fig. 1b, c). Accordingly, TREK-1-deficient neurons exhibited a lower rheobase and higher firing frequency in response to current injections (Fig. 2). Our observation is largely consistent with a previous finding in which the genetic deletion of TREK-1 alters sinoatrial node membrane excitability [33]. To the best of our knowledge, the present study has been the first in which the impact of TREK-1 deficiency on neuronal excitability has been characterized in native hippocampal neurons in brain slices.

TREK-1 Deficiency Increases Excitatory and Inhibitory Synaptic Transmission

Synaptic activity is determined and dynamically regulated by the quantity and morphology of dendritic spines [34]. Evidently, abnormal dendritic pruning and increased spine density all have been shown to increase excitatory synaptic transmission [35]. In our study, a higher mEPSCs frequency and enhanced AMPAR-EPSCs in TREK-1 KO neurons appear to account for an enhanced excitatory synaptic transmission (Fig. 4). Interestingly, TREK-1 KO also increases the strength of inhibitory synaptic transmission (Fig. 4c). It is yet unknown if an enhanced presynaptic GABA release and GABA_A receptors expression on the inhibitory postsynaptic spines would account for this observation.

Mechanistically, the facilitation of synaptic transmission should in part result from TREK-1 deficiency-induced depolarization of pre- and post-synaptic membranes. Inhibition of leak K^+ channels depolarizes synaptic terminals to facilitate Ca^{2+} influx and vesicular glutamate release [36]. In our CA1 pyramidal neuron recordings, an increased mEPSCs frequency and decreased PPR all occurred in TREK-1 KO neurons (Fig. 4a and Fig. 6a), indicating an enhanced presynaptic release probability in excitatory SC-CA1 synapses. Deletion or inactivation of voltage-gated presynaptic K^+ channels, such as Kv2 and Kv1.1, has also been shown to enhance release probability through depolarizing presynaptic membrane that facilitates Ca^{2+} influx and vesicular neurotransmitter release [37–39]. On the postsynaptic sites, TREK-1 null-induced depolarization favors the summation of EPSP events for spike generation at the axon hillock [40]. Although increased IPSCs also appeared in TREK-1 KO neurons, this postsynaptic depolarization mechanism, however, should not be applicable to the inhibitory synaptic transmission.

In synaptic failure rate analysis, a reduced failure rate and increased AMPA EPSC amplitude appear in TREK-1 KO neurons (Fig. 5c–f), favoring the view of an increase in the functional postsynaptic AMPARs. Consequently, a higher

amount of active excitatory synapses may contribute as an additional mechanism to an enhanced glutamatergic transmission in TREK-1 KO neurons. Ongoing presynaptic hyperexcitability has been speculated to downregulate postsynaptic AMPAR through homeostatic scaling [41]. Our results, however, have indicated an increased presence of functional AMPA receptors in postsynaptic terminals in TREK-1 KO neurons. Since exocytotic insertion of postsynaptic AMPARs is activity-dependent [25], we speculate that a protracted glutamatergic input (Fig. 4a) may convert more silent synapses to be the active ones in CA1 pyramidal cells. This may also explain why TREK-1 KO occluded LTP induction in SC-CA1 synapses (Fig. 6).

TREK-1 Deficiency Does Not Affect the Basic Electrophysiological Properties and Function of Astrocyte Network

Although TREK-1 channel is also expressed by astrocytes [18, 42], genetic deletion of TREK-1 did not reveal the functional contribution of this channel to the basic electrophysiological properties of astrocytes in the developing and mature brain [14, 15]. Here, we further show that TREK-1 immunoreactivity can barely be detected in astrocytes (Fig. 7a), consistent with a lack of functional TREK-1 currents in astrocytes [15]. Additionally, we showed that TREK-1 deletion exerts no impact on the function of astrocyte syncytial coupling (Fig. 7), which is critical for basic brain homeostasis and synaptic transmission [17, 28]. Nevertheless, to further differentiate the role of TREK-1 in astrocytes and neurons, cell-type specific TREK-1 gene knockout would be a better approach to answer this question in the future.

TREK-1 Null Impairs LTP and Memory

We have explored the role of TREK-1 in learning and memory at both the cellular and animal behavioral levels. At the cellular level, we observed a reduced PPR in TREK-1 KO neurons, a form of short-term plasticity determined by the probability of presynaptic glutamate release (Fig. 6a). Since depression of PPR is exclusively presynaptic, TREK-1 KO induced depolarization of presynaptic terminals and the resultant facilitation of glutamate release is likely causative.

TREK-1 KO has also shown to impair postsynaptic LTP (Fig. 6). The fact that the active excitatory synapses increase in TREK-1 KO neurons suggests a reduced pool of silent synapses. Thus, LTP occlusion in TREK-1 KO mice could be caused by a nearly saturated expression of postsynaptic AMPARs that limits further up-scaling modulation of synaptic efficacy. Such saturation of the synaptic plasticity was also found in other studies. For example, repeated seizures in the hippocampus saturate synaptic responses, preventing LTP and

impairing memory function [43]. Interestingly, TREK-1 KO mice displayed increased sensitivity to epilepsy [11].

TREK-1 is highly expressed in brain regions involved in memory and decision-making, i.e., the hippocampus and prefrontal cortex [1]. The role of TREK-1 in learning and memory has not been clearly defined. For example, TREK-1 KO was not shown to have an effect on the animal novel object recognition task [11], nor the learning/memory-associated behavioral tasks [10]. However, TREK-1 overexpression in another study exacerbated isoflurane-induced memory impairment in mice [12]. In *Drosophila*, overexpression of ork1 (a TREK-1 homolog in *Drosophila*) impairs short-term memory, whereas TREK-1 silencing attenuated the memory deficits [44]. In our animal behavior study, the altered synaptic plasticity changes are associated with a hippocampus-dependent memory deficit (Fig. 6). These discrepancies need to be reconciled in future studies.

Therapeutic Implication

Cognitive dysfunction is a major pathological feature of major depressive disorder [45]. In an animal study, TREK-1 KO mice displayed a depression-resistant phenotype [8]. Increasing evidence shows that TREK-1 blockers are highly effective antidepressants, therefore TREK-1 is considered as a promising target for depression treatment [46]. Our study indicates that TREK-1 deficiency negatively affects the LTP and memory, which raises concern about the potential clinical use of TREK-1 inhibitors. Interestingly, while the depression patients often suffer from defects in attention and memory, they also often retain and pay continued priority attention to the memory of negative information. Therefore, our results add to a growing list of evidence for a balanced evaluation of TREK-1 inhibitors for depression treatment.

Acknowledgments The authors thank Dr. Fangli Zhao for assisting the field potential recording.

Author Contributions WW and MZ conceived the project. WW, CMK, YD, AT, and XW conducted the research or assisted the research, discussed the project, and assisted the manuscript preparation. WW and MZ wrote the manuscript. MZ supervised the project. All authors are accountable for all aspects of the work and all persons designated as authors qualify for the authorship, and all those who qualify for authorship are listed. All authors read and approved the final version of the manuscript submitted for publication.

Funding Information This work was sponsored by grants from the National Institute of Neurological Disorders and Stroke R56NS097972 and RO1NS062784 (MZ), and P30NS104177 (to Dr. Candice Askwith). WW was supported by grants from the National Natural Science Foundation of China (No. 81400973) and the Fundamental Research Funds for the Central Universities of China, HUST (2018KFYYXJ081).

Compliance with Ethical Standards

All procedures performed in studies involving animals were in accordance with a protocol approved by the Animal Care and Use Committees of The Ohio State University and all efforts were made to minimize suffering. This article does not contain any studies with human participants performed by any of the authors.

Conflict of Interest The authors declare that they have no conflict of interest.

References

1. Talley EM, Solorzano G, Lei Q, Kim D, Bayliss DA (2001) CNS distribution of members of the two-pore-domain (KCNK) potassium channel family. *J Neurosci* 21(19):7491–7505
2. de la Pena E, Malkia A, Vara H, Caires R, Ballesta JJ, Belmonte C, Viana F (2012) The influence of cold temperature on cellular excitability of hippocampal networks. *PLoS One* 7(12):e52475. <https://doi.org/10.1371/journal.pone.0052475>
3. Enyedi P, Czirjak G (2010) Molecular background of leak K⁺ currents: two-pore domain potassium channels. *Physiol Rev* 90(2): 559–605. <https://doi.org/10.1152/physrev.00029.2009>
4. Honore E (2007) The neuronal background K₂P channels: focus on TREK1. *Nat Rev Neurosci* 8(4):251–261. <https://doi.org/10.1038/nrn2117>
5. Feliciangeli S, Chatelain FC, Bichet D, Lesage F (2015) The family of K₂P channels: salient structural and functional properties. *J Physiol* 593(12):2587–2603. <https://doi.org/10.1113/jphysiol.2014.287268>
6. Westphalen RI, Krivitski M, Amarosa A, Guy N, Hemmings HC Jr (2007) Reduced inhibition of cortical glutamate and GABA release by halothane in mice lacking the K⁺ channel, TREK-1. *Br J Pharmacol* 152(6):939–945. <https://doi.org/10.1038/sj.bjp.0707450>
7. Sandoz G, Levitz J, Kramer RH, Isacoff EY (2012) Optical control of endogenous proteins with a photoswitchable conditional subunit reveals a role for TREK1 in GABA(B) signaling. *Neuron* 74(6): 1005–1014. <https://doi.org/10.1016/j.neuron.2012.04.026>
8. Heurteaux C, Lucas G, Guy N, El Yacoubi M, Thummler S, Peng XD, Noble F, Blondeau N et al (2006) Deletion of the background potassium channel TREK-1 results in a depression-resistant phenotype. *Nat Neurosci* 9(9):1134–1141. <https://doi.org/10.1038/nn1749>
9. Weng W, Chen Y, Wang M, Zhuang Y, Behnisch T (2016) Potentiation of Schaffer-collateral CA1 synaptic transmission by eEF2K and p38 MAPK mediated mechanisms. *Front Cell Neurosci* 10:247. <https://doi.org/10.3389/fncel.2016.00247>
10. Mirkovic K, Palmersheim J, Lesage F, Wickman K (2012) Behavioral characterization of mice lacking Trek channels. *Front Behav Neurosci* 6:60. <https://doi.org/10.3389/fnbeh.2012.00060>
11. Heurteaux C, Guy N, Laigle C, Blondeau N, Duprat F, Mazzuca M, Lang-Lazdunski L, Widmann C et al (2004) TREK-1, a K⁺ channel involved in neuroprotection and general anesthesia. *EMBO J* 23(13):2684–2695. <https://doi.org/10.1038/sj.emboj.7600234>
12. Cai Y, Peng Z, Guo H, Wang F, Zeng Y (2017) TREK-1 pathway mediates isoflurane-induced memory impairment in middle-aged mice. *Neurobiol Learn Mem* 145:199–204. <https://doi.org/10.1016/j.nlm.2017.10.012>
13. Namiranian K, Lloyd EE, Crossland RF, Marrelli SP, Taffet GE, Reddy AK, Hartley CJ, Bryan RM Jr (2010) Cerebrovascular responses in mice deficient in the potassium channel, TREK-1. *Am J*

- Physiol Regul Integr Comp Physiol 299(2):R461–R469. <https://doi.org/10.1152/ajpregu.00057.2010>
14. Zhong S, Du Y, Kiyoshi CM, Ma B, Alford CC, Wang Q, Yang Y, Liu X et al (2016) Electrophysiological behavior of neonatal astrocytes in hippocampal stratum radiatum. *Mol Brain* 9:34. <https://doi.org/10.1186/s13041-016-0213-7>
 15. Du Y, Kiyoshi CM, Wang Q, Wang W, Ma B, Alford CC, Zhong S, Wan Q et al (2016) Genetic deletion of TREK-1 or TWIK-1/TREK-1 potassium channels does not alter the basic electrophysiological properties of mature hippocampal astrocytes in situ. *Front Cell Neurosci* 10:13. <https://doi.org/10.3389/fncel.2016.00013>
 16. Wang W, Putra A, Schools GP, Ma B, Chen H, Kaczmarek LK, Barhanin J, Lesage F et al (2013) The contribution of TWIK-1 channels to astrocyte K(+) current is limited by retention in intracellular compartments. *Front Cell Neurosci* 7:246. <https://doi.org/10.3389/fncel.2013.00246>
 17. Pannasch U, Vargova L, Reingruber J, Ezan P, Holcman D, Giaume C, Sykova E, Rouach N (2011) Astroglial networks scale synaptic activity and plasticity. *Proc Natl Acad Sci U S A* 108(20):8467–8472. <https://doi.org/10.1073/pnas.1016650108>
 18. Zhou M, Xu G, Xie M, Zhang X, Schools GP, Ma L, Kimelberg HK, Chen H (2009) TWIK-1 and TREK-1 are potassium channels contributing significantly to astrocyte passive conductance in rat hippocampal slices. *J Neurosci* 29(26):8551–8564. <https://doi.org/10.1523/JNEUROSCI.5784-08.2009>
 19. Wang W, Kiyoshi CM, Du Y, Ma B, Alford CC, Chen H, Zhou M (2016) mGluR3 activation recruits cytoplasmic TWIK-1 channels to membrane that enhances ammonium uptake in hippocampal astrocytes. *Mol Neurobiol* 53(9):6169–6182. <https://doi.org/10.1007/s12035-015-9496-4>
 20. Ferreira TA, Blackman AV, Oyrer J, Jayabal S, Chung AJ, Watt AJ, Sjostrom PJ, van Meyel DJ (2014) Neuronal morphometry directly from bitmap images. *Nat Methods* 11(10):982–984. <https://doi.org/10.1038/nmeth.3125>
 21. McKinney RA (2010) Excitatory amino acid involvement in dendritic spine formation, maintenance and remodelling. *J Physiol* 588(Pt 1):107–116. <https://doi.org/10.1113/jphysiol.2009.178905>
 22. Leger M, Quiedeville A, Bouet V, Haelewyn B, Boulouard M, Schumann-Bard P, Freret T (2013) Object recognition test in mice. *Nat Protoc* 8(12):2531–2537. <https://doi.org/10.1038/nprot.2013.155>
 23. Hille B (2001) Ion channels of excitable cells. Sinauer, Sunderland, MA
 24. Devader C, Khayachi A, Veysiere J, Moha O, Maati H, Roulot M, Moreno S, Borsotto M et al (2015) In vitro and in vivo regulation of synaptogenesis by the novel antidepressant spadin. *Br J Pharmacol* 172(10):2604–2617. <https://doi.org/10.1111/bph.13083>
 25. Kerchner GA, Nicoll RA (2008) Silent synapses and the emergence of a postsynaptic mechanism for LTP. *Nat Rev Neurosci* 9(11):813–825. <https://doi.org/10.1038/nrn2501>
 26. Liao D, Hessler NA, Malinow R (1995) Activation of postsynaptically silent synapses during pairing-induced LTP in CA1 region of hippocampal slice. *Nature* 375(6530):400–404. <https://doi.org/10.1038/375400a0>
 27. Olsen ML, Khakh BS, Skatchkov SN, Zhou M, Lee CJ, Rouach N (2015) New insights on astrocyte ion channels: critical for homeostasis and neuron-glia signaling. *J Neurosci* 35(41):13827–13835. <https://doi.org/10.1523/JNEUROSCI.2603-15.2015>
 28. Ma B, Buckalew R, Du Y, Kiyoshi CM, Alford CC, Wang W, McTigue DM, Enyeart JJ et al (2016) Gap junction coupling confers isopotentiality on astrocyte syncytium. *Glia* 64(2):214–226. <https://doi.org/10.1002/glia.22924>
 29. Kiyoshi CM, Du Y, Zhong S, Wang W, Taylor AT, Xiong B, Ma B, Terman D et al (2018) Syncytial isopotentiality: a system-wide electrical feature of astrocytic networks in the brain. *Glia* 66(12):2756–2769. <https://doi.org/10.1002/glia.23525>
 30. Hocking JC, Pollock NS, Johnston J, Wilson RJ, Shankar A, McFarlane S (2012) Neural activity and branching of embryonic retinal ganglion cell dendrites. *Mech Dev* 129(5-8):125–135. <https://doi.org/10.1016/j.mod.2012.05.003>
 31. Frangeul L, Kehayas V, Sanchez-Mut JV, Fievre S, Krishna KK, Pouchelon G, Telley L, Bellone C et al (2017) Input-dependent regulation of excitability controls dendritic maturation in somatosensory thalamocortical neurons. *Nat Commun* 8(1):2015. <https://doi.org/10.1038/s41467-017-02172-1>
 32. Kasai H, Matsuzaki M, Noguchi J, Yasumatsu N, Nakahara H (2003) Structure-stability-function relationships of dendritic spines. *Trends Neurosci* 26(7):360–368. [https://doi.org/10.1016/S0166-2236\(03\)00162-0](https://doi.org/10.1016/S0166-2236(03)00162-0)
 33. Unudurthi SD, Wu X, Qian L, Amari F, Onal B, Li N, Makara MA, Smith SA et al (2016) Two-pore K+ channel TREK-1 regulates sinoatrial node membrane excitability. *J Am Heart Assoc* 5(4):e002865. <https://doi.org/10.1161/JAHA.115.002865>
 34. Yuste R, Bonhoeffer T (2001) Morphological changes in dendritic spines associated with long-term synaptic plasticity. *Annu Rev Neurosci* 24:1071–1089. <https://doi.org/10.1146/annurev.neuro.24.1.1071>
 35. Zhou YD, Lee S, Jin Z, Wright M, Smith SE, Anderson MP (2009) Arrested maturation of excitatory synapses in autosomal dominant lateral temporal lobe epilepsy. *Nat Med* 15(10):1208–1214. <https://doi.org/10.1038/nm.2019>
 36. Lauritzen M, Dreier JP, Fabricius M, Hartings JA, Graf R, Strong AJ (2011) Clinical relevance of cortical spreading depression in neurological disorders: migraine, malignant stroke, subarachnoid and intracranial hemorrhage, and traumatic brain injury. *J Cerebr Blood Flow Metab* 31(1):17–35. <https://doi.org/10.1038/jcbfm.2010.191>
 37. Geiger JR, Jonas P (2000) Dynamic control of presynaptic Ca(2+) inflow by fast-inactivating K(+) channels in hippocampal mossy fiber boutons. *Neuron* 28(3):927–939
 38. Yang CT, Lu GL, Hsu SF, MacDonald I, Chiou LC, Hung SY, Chen YH (2018) Paeonol promotes hippocampal synaptic transmission: the role of the Kv2.1 potassium channel. *Eur J Pharmacol* 827:227–237. <https://doi.org/10.1016/j.ejphar.2018.03.020>
 39. Gu J, Lee CW, Fan Y, Komlos D, Tang X, Sun C, Yu K, Hartzell HC et al (2010) ADF/cofilin-mediated actin dynamics regulate AMPA receptor trafficking during synaptic plasticity. *Nat Neurosci* 13(10):1208–1215. <https://doi.org/10.1038/nn.2634>
 40. Malik R, Johnston D (2017) Dendritic GIRK channels gate the integration window, plateau potentials, and induction of synaptic plasticity in dorsal but not ventral CA1 neurons. *J Neurosci* 37(14):3940–3955. <https://doi.org/10.1523/JNEUROSCI.2784-16.2017>
 41. Turrigiano GG (2017) The dialectic of Hebb and homeostasis. *Philos Trans R Soc Lond Ser B Biol Sci* 372(1715). <https://doi.org/10.1098/rstb.2016.0258>
 42. Cahoy JD, Emery B, Kaushal A, Foo LC, Zamanian JL, Christopherson KS, Xing Y, Lubischer JL et al (2008) A transcriptome database for astrocytes, neurons, and oligodendrocytes: a new resource for understanding brain development and function. *J Neurosci* 28(1):264–278. <https://doi.org/10.1523/JNEUROSCI.4178-07.2008>
 43. Gilbert TH, McNamara RK, Corcoran ME (1996) Kindling of hippocampal field CA1 impairs spatial learning and retention in the Morris water maze. *Behav Brain Res* 82(1):57–66
 44. Zhang X, Zheng Y, Ren Q, Zhou H (2017) The involvement of potassium channel ORK1 in short-term memory and sleep in

- Drosophila. *Medicine* 96(27):e7299. <https://doi.org/10.1097/MD.0000000000007299>
45. Zuckerman H, Pan Z, Park C, Brietzke E, Musial N, Shariq AS, Iacobucci M, Yim SJ et al (2018) Recognition and treatment of cognitive dysfunction in major depressive disorder. *Front Psychiatry* 9:655. <https://doi.org/10.3389/fpsy.2018.00655>
 46. Djillani A, Pietri M, Mazella J, Heurteaux C, Borsotto M (2019) Fighting against depression with TREK-1 blockers: past and future.

A focus on spadin *Pharmacology & Therapeutics* 194:185-198. doi: <https://doi.org/10.1016/j.pharmthera.2018.10.003>

Publisher's Note Springer Nature remains neutral with regard to jurisdictional claims in published maps and institutional affiliations.